



ORIGINAL ARTICLE

Behavior of CFA and H-section steel piles in lateral loading: experimental and numerical analysis

Comportamento de estacas escavadas em hélice contínua (CFA) e de estacas metálicas em seção H sob carregamento lateral: análise experimental e numérica

Alex Micael Dantas de Sousa^a Yuri Daniel Jatobá Costa^b Arthur Gomes Dantas de Araujo^c Carina Maia Lins Costa^b ^aUniversidade de São Paulo – USP, Escola de Engenharia de São Carlos, Departamento de Engenharia de Estruturas, São Carlos, SP, Brasil^bUniversidade Federal do Rio Grande do Norte – UFRN, Departamento de Engenharia Civil, Natal, RN, Brasil^cUniversidade Federal Rural do Semi-Árido – UFERSA, Departamento de Engenharia Civil, Angicos, RN, Brasil

Received 16 June 2020

Accepted 26 September 2020

Abstract: The behavior of continuous flight auger (CFA) piles and steel H-section piles to lateral loading is investigated using numerical analyses supported by field tests. A three-dimensional finite element numerical model to lateral load is presented. The numerical model was validated with the results of twelve lateral load tests performed on CFA and steel H-section piles installed in two deposits of sandy soils. The three-dimensional approach proposed in this study is in good agreement with the response observed with the field tests, and thus represents a reliable soil-pile interaction for laterally loaded piles in sandy soil. Parametric analyses were used to assess the influence of relevant variables to lateral soil-pile interaction. Major findings of this paper indicate that the ultimate lateral load of short rigid piles is considerably more influenced by changes in soil-pile relative stiffness than that of long flexible units. Pile diameter and soil-pile interface friction are found to exert a marked effect on the lateral load of CFA piles, while soil dilatancy is found to play a minor influence on the response of CFA piles.

Keywords: laterally loaded pile, soil-pile interaction, three-dimensional finite element method, field test, p-y curve.

Resumo: O comportamento de estacas escavadas com trado em hélice contínua (CFA) e estacas metálicas de seção H sujeitas à cargas horizontais é investigado através de análises numéricas baseadas em resultados experimentais. O modelo numérico foi validado com os resultados de 12 ensaios de carregamento lateral de estacas realizados em estacas CFA e estacas metálicas de seção H instaladas em duas regiões de solos arenosos. A abordagem tridimensional proposta neste estudo está de acordo com a resposta observada nos ensaios de campo e, portanto, representa uma interação solo-estaca confiável para estacas carregadas lateralmente em solo arenoso. Análises paramétricas foram utilizadas para avaliar a influência de variáveis relevantes para a interação lateral solo-estaca. As principais descobertas deste trabalho indicam que a capacidade de carga lateral última de estacas rígidas curtas é consideravelmente mais influenciada por mudanças na rigidez relativa do solo-estaca do que no caso de estacas flexíveis longas. O diâmetro da estaca e o atrito da interface solo-estaca tem efeito significativo na capacidade de carga lateral das estacas CFA, enquanto a dilatação do solo exerce uma menor influência na resposta destas.

Palavras-chave: estacas carregadas lateralmente, interação solo-estaca, método dos elementos finitos tridimensional, ensaios de campo, curva p-y.

How to cite: A. M. D. Sousa, Y. D. J. Costa, A. G. D. Araujo, and C. M. L. Costa, “Behavior of CFA and H-section steel piles in lateral loading: experimental and numerical analysis,” *Rev. IBRACON Estrut. Mater.*, vol. 14, no. 3, e14313, 2021, <https://doi.org/10.1590/S1983-41952021000300013>

Corresponding author: Alex Micael Dantas de Sousa. E-mail: alex_dantas@usp.br

Financial support: Fundação de Amparo à Pesquisa do Estado de São Paulo, Grant/Award Number: FAPESP - 2018/21573-2; Conselho Nacional de Desenvolvimento Científico e Tecnológico.

Conflict of interest: Nothing to declare.



This is an Open Access article distributed under the terms of the Creative Commons Attribution License, which permits unrestricted use, distribution, and reproduction in any medium, provided the original work is properly cited.

1 INTRODUCTION

Soil-structure interaction has been extensively investigated regarding axial vertical loads in deep foundations [1]–[3]. At the same time, in several circumstances, piles need to be designed to support major lateral loads, as a result of the action of wind, water flow, horizontal earth pressure [4], earthquakes, and traffic movement. Bridges [5], tall buildings, transmission lines, retaining walls [4], offshore structures [6]–[8], wharfs [9], are a few examples of structures in which lateral loads assume primary significance.

Among existing methods for the analysis of laterally loaded single piles, p – y curve methods are largely employed in current design practice. In the p – y curve approach, a laterally loaded pile is treated as a beam on an elastic foundation with independent springs. The soil resistance per unit length (p) is assumed to hold a non-linear relationship with the pile lateral displacement (y). The relationship between p and y is known as the subgrade reaction modulus k_h ($k_h = p/y$). The soil-pile system is assumed to reach the ultimate lateral resistance at a particular pile deflection level. The non-linearity between soil resistance and pile displacement has been substantiated by numerous full-scale tests [5], [10]–[14].

Although versatile and practical for structural design purposes, the p – y curve approach has several shortcomings, such as: (1) continuity of the soil is not accounted for, since the springs are uncoupled; (2) shearing forces in the pile-soil contact and pile toe are neglected; (3) pile diameter and bending stiffness are only considered indirectly; (4) soil dilatancy is neglected, even though experimental evidence reveals that pile-soil resistance can significantly increase with increasing soil dilatancy [12], [15]; (5) the soil-pile ultimate resistance (p_u) is calculated according to Rankine's theory, which assumes full slippage conditions between the soil and the structure [16], [17], even though perfectly smooth conditions are not found in the field; (6) the coefficient of horizontal earth pressure (K) is considered equal to the at-rest earth pressure coefficient (K_0) rather than the post-installation earth pressure coefficient, which may result in underestimated ultimate soil resistances for piles [12], [18], [19].

An alternative to the p – y curve approach is the three-dimensional finite element method (3-D FEM) analysis. Although comparatively more complex to implement, 3-D FEM can reliably simulate several aspects of the problem involving a laterally loaded pile that are unable to be accomplished in p – y curve methods. 3-D FEM methods should be preferred over p – y curve methods because they are more rigorous in their analytical methodology.

Many numerical studies have been extensively conducted to assess the behavior of piles under lateral loading. Although several studies used 3-D FEM analysis supported by field data [5], [12], [15], [20]–[22], some relevant aspects of the problem involving laterally loaded pile behavior have not been well understood.

For instance, while the effect of the pile bending stiffness on pile response has been widely investigated in the literature [12], [23], [24], very little importance has been granted to the soil-pile relative stiffness, even though this variable is comparatively more suitable for describing the soil-pile interaction. Moreover, different studies present contradictory conclusions on the influence of pile diameter on the lateral behavior of piles, which warrants further research. Terzaghi [25] and Vesic [26] postulated that the pile diameter did not influence the subgrade reaction modulus (k_h). Using numerical and large-scale tests, Ashford and Juirnarongrit [27] and Fan and Long [12] verified that the pile diameter has an insignificant influence on k_h . However, other investigations involving experimental and analytical components found that k_h and the ultimate lateral capacity (H_u) increase linearly with the pile diameter [5], [23], [28].

Another parameter of interest for the soil-pile interaction that needs further examination is the soil-pile interface property (interface friction for granular soils or interface adhesion for non-granular soils). From a FEM analysis validated against field tests, Choi et al. [15] found that the soil-pile interface friction coefficient had a great impact on the lateral load capacity of bored piles embedded in weathered granite soil. On the other hand, the computational results presented by Kim and Jeong [5] indicated that the interface adhesion exerts an insignificant influence on the subgrade reaction modulus obtained with large diameter piles in clay.

Perceived gaps and conflicting results in the literature support the need for additional research using reliable 3-D FE models. The purpose of this study is to present the results of a 3-D FE model developed to represent the lateral load behavior of concrete flight auger (CFA) piles and steel H-section piles installed in two profiles of sandy soils. Accuracy of the proposed model was checked against the results of a total of 12 lateral load tests performed in the field with both CFA piles and steel H-section piles. Parametric analyses were carried out to investigate the influence of (i) soil-pile relative stiffness, (ii) pile diameter, (iii) interface friction between the pile and the soil and (iv) soil dilatancy. Therefore, this study brings together experimental and numerical results that provide important background for the future preliminary design of piles under lateral loading in similar soil conditions.

2 SITE CHARACTERISTICS

The experimental component of this investigation was carried out at a site located in the City of Natal (05°47'42"S, 35°12'34"W), in the Northeast region of Brazil (Figure 1a). Tertiary and quaternary sediments compose the subsoil of Natal, which is typical of vast extensions of the upper Brazilian northeast region. The tertiary deposits comprise a continuous sequence of clastic sediments, ranging from clay to conglomerate, which presents lateritic features with iron oxides bonding the soil particles together [29]. Overlying the tertiary deposits are quaternary deposits of eolian (dune) and alluvial sediments, composed of quartz sands with sub-rounded fine to coarse grains. Specifically, the experimental site is in a deflation zone composed of sandy soils of eolian origin, with grain size distribution containing less than 20% of finer sediments.

The field tests were conducted in two different locations within the experimental site, which are labeled in this study as testing Area A and testing Area B. The distance between both locations within the experimental site is approximately 300 m. The experimental site was characterized by field and laboratory tests. The field survey included four standard penetration tests (SPT) and one piezocone (CPT_u) test in each area of investigation. Subsoil profiles of Areas A and B are schematically shown in Figure 1b and Figure 1c, respectively, which include the variation with depth of the mean SPT blow count corrected for 60% efficiency (N_{60}), the cone tip resistance (q_c), and the friction ratio (R_f). Groundwater level was not detected during borehole logging. The water table is usually encountered at great depths below the ground surface (> 50 m). Surveying in Area B was performed before the placement of the surficial backfill layer.

In both areas, the surficial soil layer is composed of a 3-m-thick pure sand backfill, collected from a neighboring cut sector within site. Below the backfill sand lay natural layers of dune sediments, composed of sand and silty sand. The backfill is a medium uniformly graded quartz silica sand of eolian origin that classifies as SP, according to the Unified Soil Classification System. The grain size distribution of the backfill sand is shown in Figure 2a. The sand has an average particle size of 0.35 mm, a coefficient of uniformity of 2.2, and a coefficient of curvature of 1.07. The sand has less than 2% of the particles finer than 0.075 mm and more than 98% finer than 2 mm. Its specific gravity is 2.59, and maximum and minimum void ratios are 0.83 and 0.60, respectively. The top sand layer was compacted with relative density (D_r) of 45% in Area A, and 70% in Area B. Controlled compaction in the field was carried out using vibrating drum rollers.

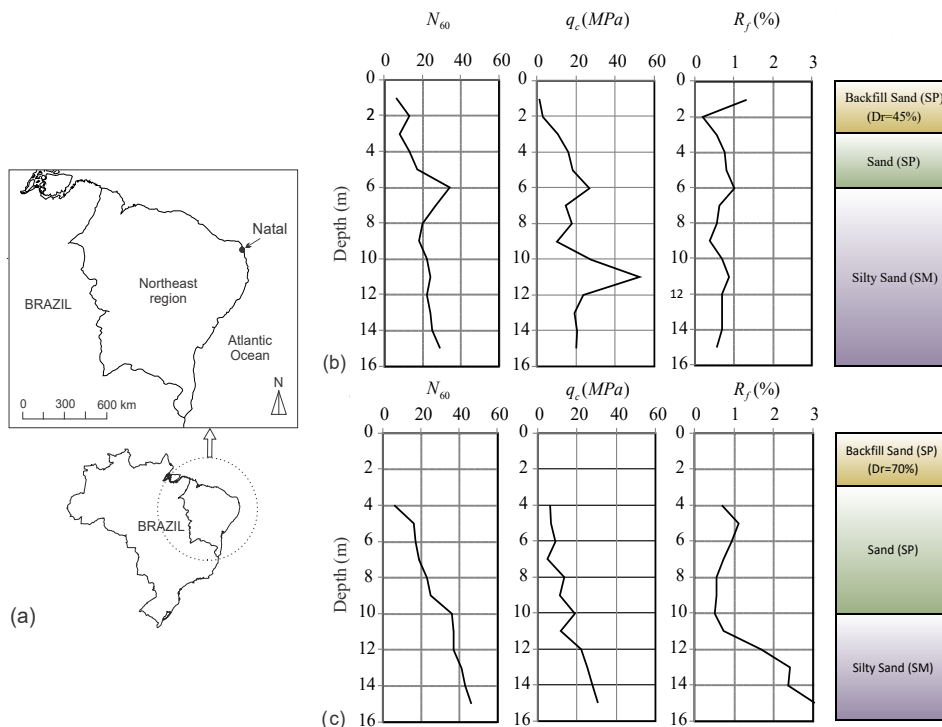


Figure 1. (a) Location of test site; (b) Site investigation results in Area A; (c) Site investigation results in Area B.

Shear strength parameters of the backfill sand were obtained from two series of conventional CID triaxial compression tests carried out with confining effective stresses (σ'_3) of 50 kPa, 100 kPa, and 200 kPa. One series of tests was prepared with target relative density (D_r) of 45%, and another series was prepared with $D_r = 70\%$, which are the same densities used in the field. Peak friction angle (ϕ'_p) was calculated from the K_f line of p - q diagrams of the tested soil. Values of ϕ'_p equals 33.6° and 38.1° for $D_r = 45\%$ and 70% , respectively. Deviator stress-axial strain and volume change behavior for the soil at the relative density of 45% are presented in Figure 2b and Figure 2c, respectively, and the corresponding K_f line is indicated in Figure 2d.

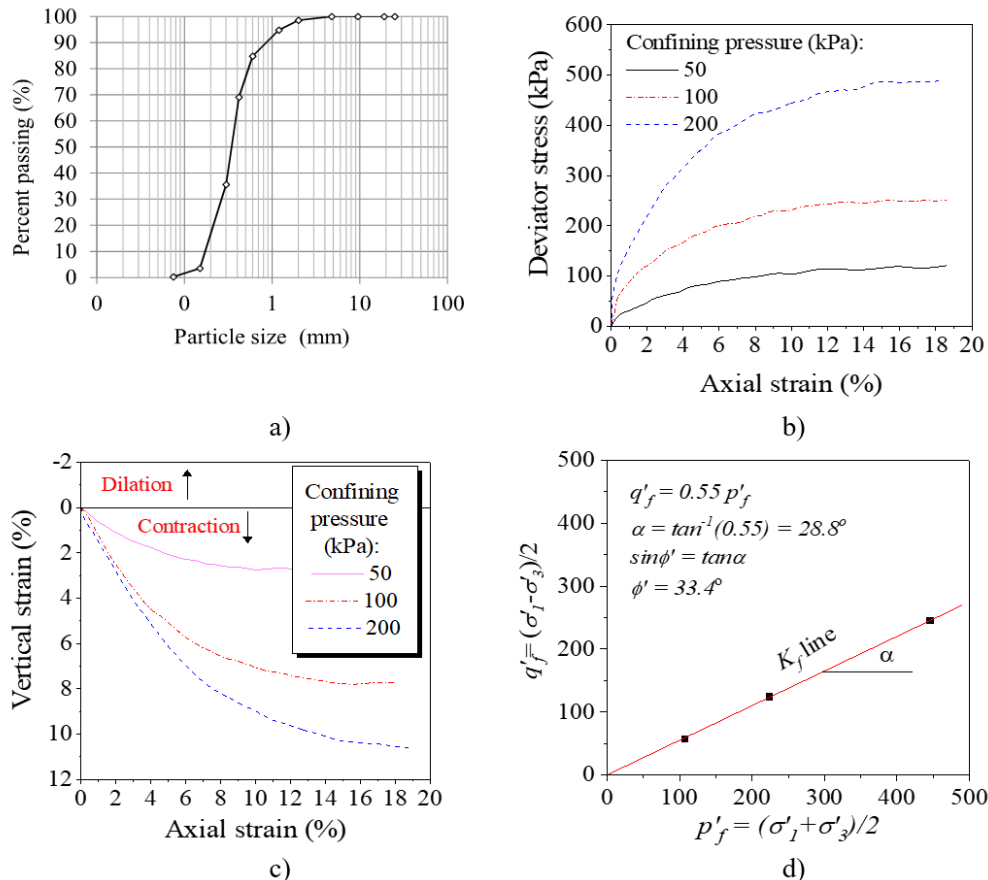


Figure 2. Properties of the backfill sand: (a) grain-size distribution; (b-c) results of CID triaxial tests performed on sand samples prepared with a relative density of 45%; (d) p - q diagram of the tested sand.

3 FIELD TESTING PROGRAM AND INSTRUMENTATION

A total of 12 field load tests were carried out to investigate the lateral behavior of single piles in the two sandy soil profiles. Continuous flight auger (CFA) and steel H-section model piles were installed in Areas A and B, as indicated in Figure 3. The tests were performed simultaneously on two piles with identical lengths and cross-sections, which reacted against each other. As shown in Figure 3, piles CFA-i and CFA-ii were tested together, and so did piles HS1-i and HS1-ii, and HS2-i and HS2-ii. A summary of the testing sequence is presented in Table 1, which indicates the pile type, the area where the test was carried out, and the test designation.

The CFA piles were cast with a diameter (D) of 0.6 m and length (L) of 10 m. The integrity of the CFA piles was verified by a low-strain integrity test that uses the pulse-echo method, commonly named as pile integrity test (PIT). The reinforcement of the CFA piles consists of 10 longitudinal steel bars with 20 mm in diameter enveloped by a steel spiral with 8.0 mm in diameter and 200 mm in spacing. Concrete with characteristic compressive strength of 35 MPa at 28 days was used for the CFA piles. The initial flexural stiffness ($E_p I_p$) of the CFA pile cross-section is 220 MN m².

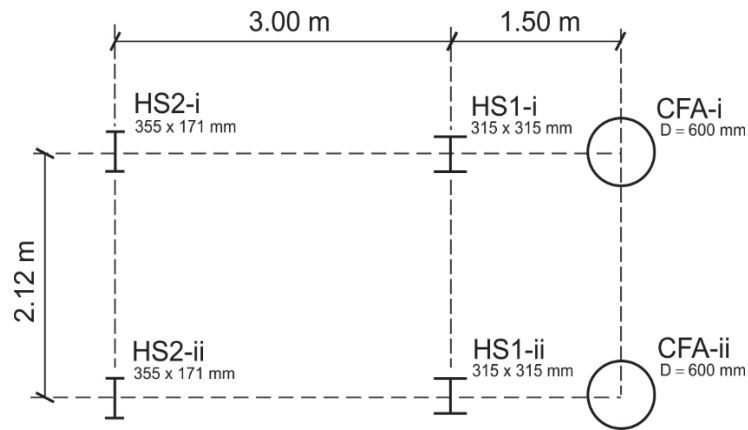


Figure 3. Elevation view showing the position of model piles.

Table 1. Testing program summary

Test N°	Pile type	Testing Area	Backfill relative density, D_r (%)	Designation
1	CFA	B	70	CFA-B-70-i
2	CFA	B	70	CFA-B-70-ii
3	CFA	A	45	CFA-A-45-i
4	CFA	A	45	CFA-A-45-ii
5	HS1	A	45	HS1-A-45-i
6	HS1	A	45	HS1-A-45-ii
7	HS2	A	45	HS2-A-45-i
8	HS2	A	45	HS2-A-45-ii
9	HS2	B	70	HS2-B-70-i
10	HS2	B	70	HS2-B-70-ii
11	HS1	B	70	HS1-B-70-i
12	HS1	B	70	HS1-B-70-ii

Two different steel H-section piles were used, as shown in Figure 3. One pair of steel piles had cross-section with width = 315 mm, height = 315 mm, flange thickness = 17.4 mm and web thickness = 17.4 mm (HS1-i and HS1-ii). The other pair of steel piles had cross-section with width = 171 mm, height = 355 mm, flange thickness = 11.6 mm and web thickness = 7.2 mm (HS2-i and HS2-ii). All steel piles had a total length of 6 m and embedded length in the ground of 4.5 m. The initial bending stiffness ($E_p I_p$) of the cross-section of piles HS1 and HS2 are 56 MN.m² and 29 MN.m², respectively.

In both testing areas, HS1 and HS2 piles were tested before the casting of the CFA piles. Spacing between the CFA and the HS1 pairs of piles (Figure 3) was defined to accommodate the use of these piles as a reaction for a vertical load test performed in another pile installed after completion of the lateral load tests, which is not included in the present study. The distance between HS1 and CFA piles was assumed sufficient to minimize cross-interference. Based on experimental results from physical model tests, Davisson [30] concluded there is essentially no influence of one pile on another, providing the spacing normal to the direction of loading is at least 2.5 D from the pile axis. According to results from instrumented tests on small-scale models of laterally loaded piles, at a depth of 3.45 D below the soil surface, horizontal stress changes extend to a maximum distance of 2.5 D beside the pile [31].

The layout of the installation and instrumentation of the CFA model piles is depicted in Figure 4a. A shallow pit with a depth of 0.5 m was excavated between the piles to accommodate the loading system. The load was applied in cumulative equal increments using a hydraulic cylinder with a maximum nominal capacity of 500 kN. The cylinder was positioned as close as possible to the pile head. Load measurements were obtained by a calibrated load cell with a maximum nominal capacity of 500 kN. Horizontal pile displacements (y_i) were recorded at the ground surface level

using dial gages with a resolution of 0.01 mm and a maximum stroke of 50 mm. The dial gauges were mounted in magnetic-articulated bases set on two steel reference beams.

Similar instrumentation, as described above, was used in the tests with the steel piles, and a general scheme of its setup is illustrated in Figure 4b. The loading system was mounted directly on the ground surface, and the horizontal displacements of the pile (y_i) were recorded at 0.5 m and 1.2 m above the ground surface.

All lateral loading tests were performed with static quick maintained load (QML) [32] and followed the Brazilian code ABNT NBR 12131:2006 [33]. Each load increment was held constant for 5 min, and displacement readings were taken at every minute. The unloading phase was carried out with four 5-minute-long decrements. The unloading stages were not recorded in Test 5 due to the sudden disassembling of the loading system during the last stage.

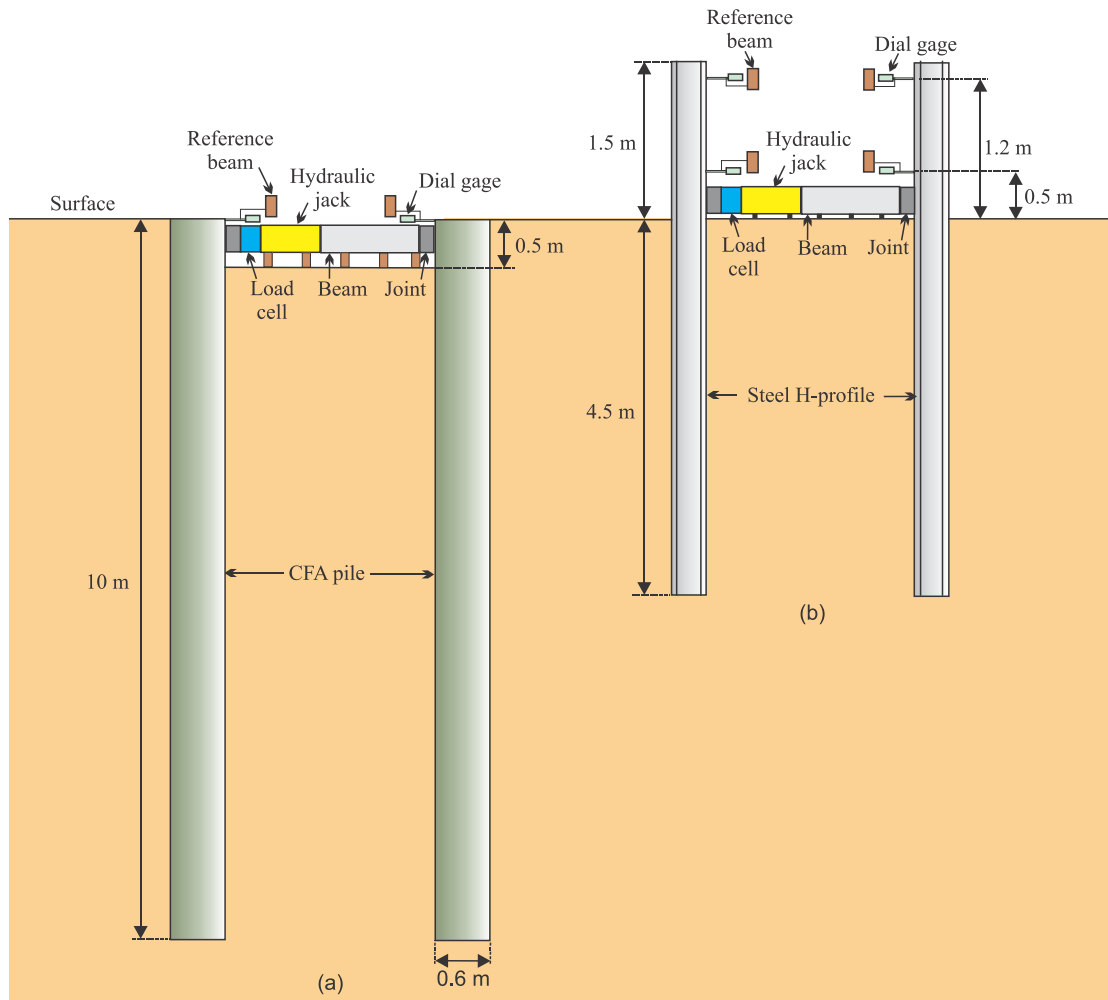


Figure 4. General scheme of testing assemblage and used apparatus: (a) CFA piles; (b) steel H-section piles.

4 FIELD TEST RESULTS

Figure 5 shows the lateral applied load (H) versus measured lateral displacement (y_i) curves of each individual pile, obtained from the field tests performed in Areas A and B. The displacements (y_i) recorded with the upper dial gages in the tests with the steel H-section profiles are omitted from Figure 5 for clarity. By comparing the results of the same pair of piles, it is possible to notice that the curves of the steel H-section piles situate within a narrower range than those of the CFA piles. Imperfections in the shaft of the CFA piles associated with the construction process may partially explain the poorer repeatability of the tests with this pile type since no cast-in-place pile is exactly equal to another.

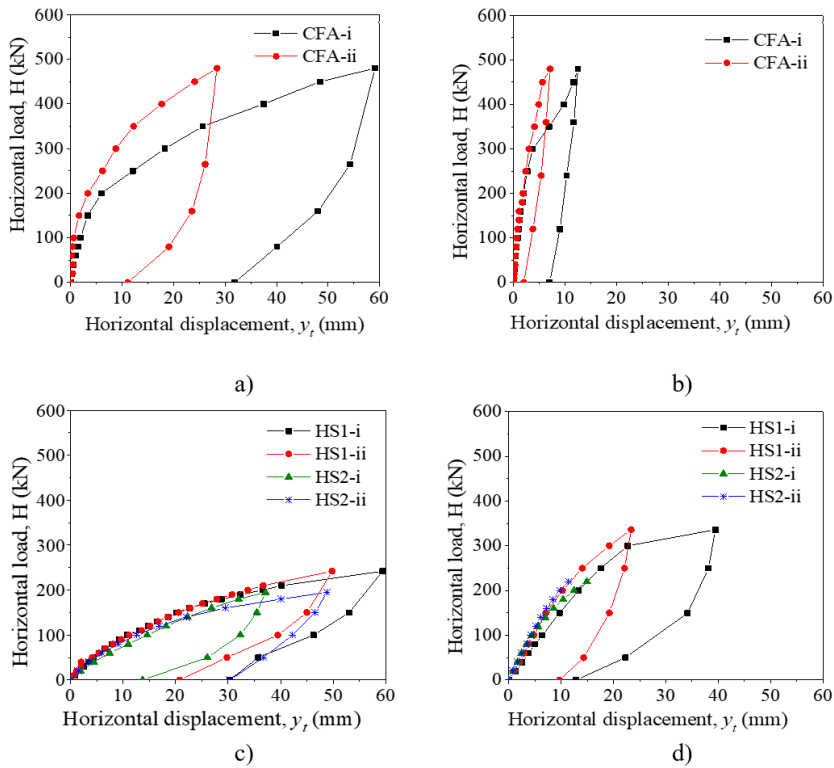


Figure 5. Results of the lateral tests: (a) CFA piles in Area A; (b) CFA piles in Area B; (c) steel H-section piles in Area A; (d) steel H-section piles in Area B.

The CFA piles reached larger maximum lateral loads in comparison to the steel piles. The average value of the maximum horizontal load with the CFA piles was 480 kN in both testing areas, which is close to the limit load of 500 kN of the loading system. In Area A, the average value of the maximum horizontal load of pair HS1 was 242 kN, and of the pair HS2 was 195 kN. Slightly higher maximum lateral loads were obtained with the steel piles installed in Area B due to the greater relative density of the sand backfill: 334 kN with pair HS1 and 220 kN with pair HS2. The unloading portion of the curves reveals that the horizontal displacement recovered after unloading is significant and is larger with the steel piles than the CFA piles, due to the resilient feature of the steel.

In both testing areas, the results of the HS1 and HS2 piles were close. As expected, the curves of the HS1 piles showed slightly larger horizontal loads for a specific displacement, due to the higher cross-section flexural stiffness of that pile type.

The constant of horizontal subgrade reaction (n_h) was back calculated from the load test results of the CFA piles using the following equation [22]:

$$y_0 = 2,435H \frac{T^3}{E_p I_p} + 1,623(He) \frac{T^2}{E_p I_p} \tag{1}$$

where: y_0 = horizontal displacement of the pile at the ground surface; H = horizontal applied load; e = position of the axis of application of H above the ground surface; E_p = Young’s modulus of pile material; I_p = moment of inertia of pile cross-section; T = pile characteristic length, given as:

$$T = \sqrt[5]{\frac{E_p I_p}{n_h}} \tag{2}$$

Since the displacements of the CFA piles were recorded at the level of the terrain, Equation 1 was solved assuming $y_0 = y_t$. The characteristic length T was obtained from Equation 1 assuming the distance from the ground surface to the point of application of the load (e) equals zero. After finding the characteristic length, n_h was calculated from Equation 2.

The constant of horizontal subgrade reaction of the steel H-section piles was calculated by solving a system composed of Equations 1 and 3, which gives T , $E_p I_p$, and y_0 for each applied load H .

$$y_0 = y_t + S_0(e + e') - \frac{He^3}{3E_p I_p} - \frac{He^2 e'}{2E_p I_p} \tag{3}$$

where: y_t = mean horizontal displacement of piles tested simultaneously against each other; S_0 = rotation of the pile head at the ground surface; e' = vertical distance from the axis of application of H to the position of measurement of y_t . In the assemblage of the tests with the steel H-section piles, $e = 0.2$ m, and $e' = 0.3$ m or 1 m (see Figure 4).

The rotation of the pile head at the ground surface was calculated from Matlock and Reese [34]:

$$S_0 = -1.623H \frac{T^2}{E_p I_p} - 1.750He \frac{T}{E_p I_p} \tag{4}$$

This approach for the computation of n_h assumes that the modulus of subgrade reaction, obtained for the soil near the surface of the terrain, varies linearly with depth and is representative of the entire ground along the pile length. However, potential inaccuracies produced by this assumption are not supposed to be significant, since it is well established that the response of a pile to lateral loading is essentially controlled by the stiffness of the soil at shallow depth [13], [35]. Zhang et al. [36] reported depths of influence between 3 and 4 times the pile diameter. Considering the soil profile of the present study, such depth of influence is within the surficial sand layer, which suggests that the pile response is ruled by this layer.

Figure 6a and Figure 6b show the relationship between n_h and the horizontal displacement y_0 obtained for Areas A and B, respectively. The horizontal displacement y_0 is normalized by dimension B , which is the diameter of the CFA pile or the width of the steel pile. The constant of horizontal subgrade reaction follows a steep decrease at small horizontal displacements and tends to stabilize with increasing displacements. Values of n_h were significantly larger with the denser backfill sand of Area B. As pointed out by Prakash and Kumar [37] the modulus of horizontal reaction depends strongly on the relative density of sands.

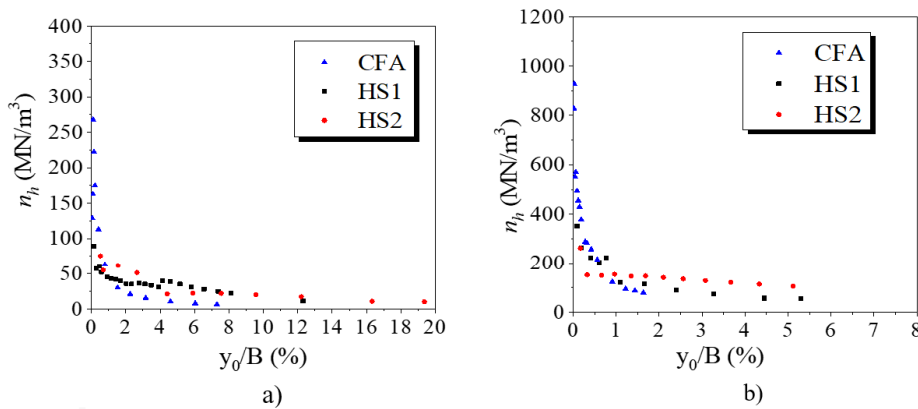


Figure 6. Relationship between the constant of subgrade reaction n_h and the horizontal pile displacement at ground level: (a) Area A; (b) Area B.

5 THREE-DIMENSIONAL NUMERICAL MODELING OF LATERALLY LOADED CFA AND STEEL H-SECTION PILES

The finite-element program Plaxis3D was used to simulate the response of a single pile under lateral load in the studied soil profiles. Figure 7a and Figure 7b show the typical undeformed 3-D FE mesh used in the analyses of the CFA piles. The model boundaries extended to a width of 10 m from the pile center and to a depth equal to 20 m (*i.e.*,

the pile length plus 10 m below the pile-toe level). These dimensions were considered sufficient to exclude boundary effects in previous investigations. The outer vertical boundary of the mesh is fixed in the horizontal direction and free in the vertical direction. The base of the soil model is constrained in both vertical and horizontal directions. The mesh consists of 15-node wedge elements, which were applied to simulate both the soil and the CFA pile. The meshing discretization used in this study followed the approach proposed by Kim and Jeong [5]. For the proposed numerical model, the mesh was manually refined close to the pile. Although one dimension of the elements in the vicinity of the pile is considerably smaller than the other two (i.e., elements with large aspect ratio, as shown in Figure 7c), the use of wedge elements with quadratic approximation (15 nodes) reduced potential numerical problems of convergence. Moreover, since the mean size of the element cannot be freely defined in the software, refinement of the mesh close to the pile was necessary to ensure a higher number of elements and nodes in the loading direction.

All numerical simulations were carried out under drained conditions. The soil behavior was modeled by the hardening soil (HS) constitutive model developed under the framework of the theory of plasticity, in which a stress-strain relationship, due to the primary loading, is assumed to be a hyperbolic curve [38]. Soil failure takes place according to the Mohr-Coulomb failure criterion. The CFA pile was considered as an isotropic linear-elastic material. The material properties of soils and piles used in this analysis are depicted in Table 2.

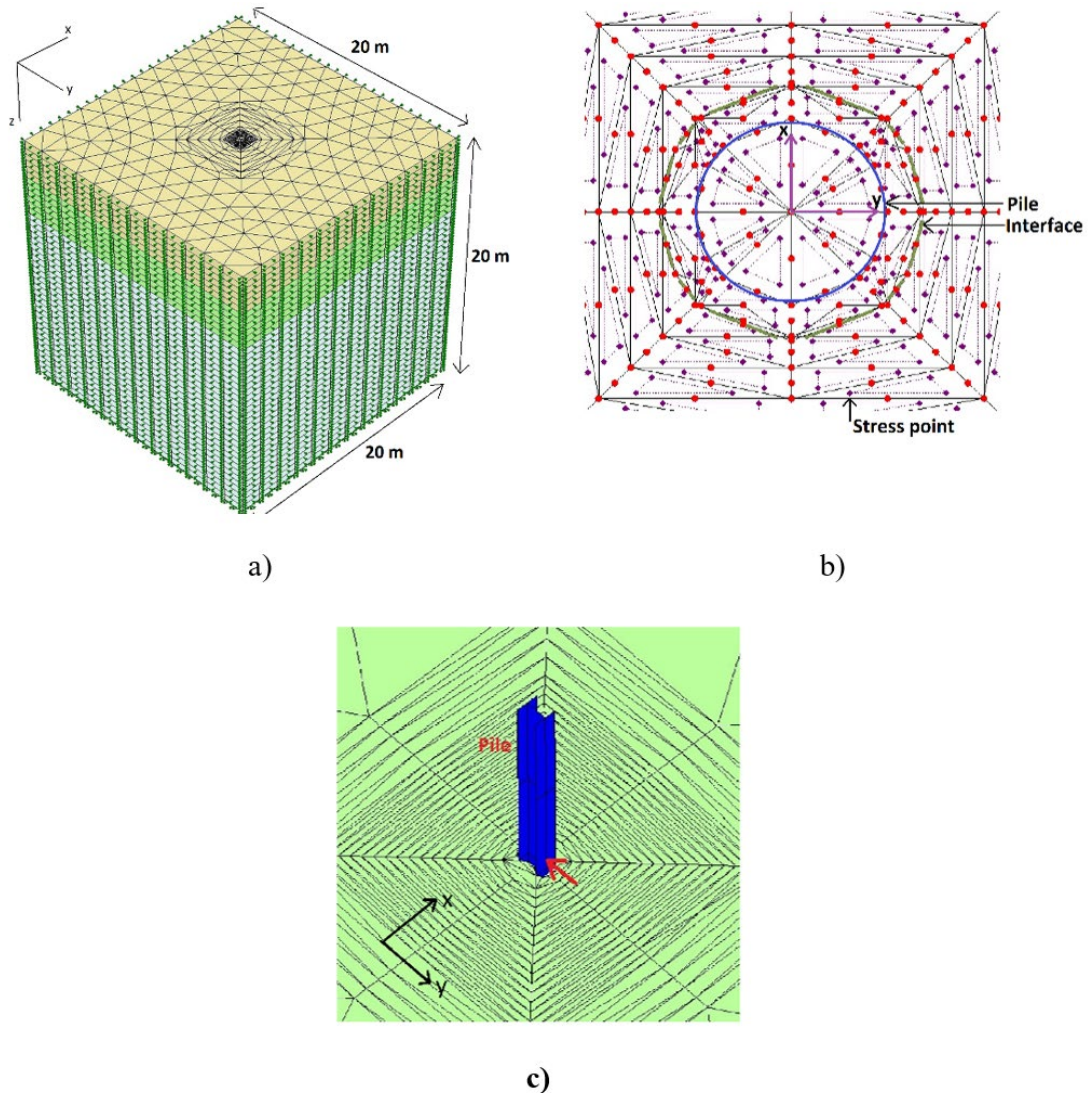


Figure 7. Three-dimensional finite-element mesh: (a) 3D view of CFA pile model; (b) cross-section in x-y plane of CFA pile model; (c) surface view of steel H-section HS1 pile model.

Table 2 - Material properties used in the FE analysis

Material		Parameter			
CFA pile	Concrete unit weight, γ (kN/m ³)	25			
	Pile Young's modulus, E_p (MPa)	35,000			
	Pile coefficient of Poisson, ν_p	0.2			
H-Steel pile	Pile Young's modulus, E_p (MPa)	207,000			
Soil		Backfill	Sand	Silty Sand	
Area A ($D_r = 45\%$)	Soil unit weight, γ (kN/m ³)	16	17.5	17	
	Soil Young's modulus, E_s (MPa)	50	100	100	
	Soil coefficient of Poisson, ν_s	0.30	0.35	0.35	
	Peak friction angle, ϕ'_p (°)	31.6	38	36.4	
	Soil-pile interface friction angle, δ (°)	22.3	27.5	26.2	
	Effective cohesion, c' (kPa)	5	5	10	
	Dilatancy angle, ψ (°)	0	5	10	
	Area B ($D_r = 70\%$)	Soil unit weight, γ (kN/m ³)	18	17	18
		Soil Young's modulus, E_s (MPa)	100	100	100
		Soil coefficient of Poisson, ν_s	0.35	0.35	0.35
Peak friction angle, ϕ'_p (°)		35.1	37	40.6	
Soil-pile interface friction angle, δ (°)		25.1	26.7	29.7	
Effective cohesion, c' (kPa)		5	5	10	
	Dilatancy angle, ψ (°)	10	5	10	

The main parameter governing the soil-pile interface properties in Plaxis software is the strength reduction factor (R_{inter}), which is the ratio between interface friction coefficient ($\mu_{inter} = \tan\delta$) and soil friction coefficient ($\mu = \tan\phi'$) or the ratio between interface cohesion (c_{inter}) and soil cohesion (c'). R_{inter} varies between 0 and 1. The baseline R_{inter} value used in the present study is 0.7.

The steel H-section piles were modeled using plate elements with prescribed flexural and axial rigidities. The models with the steel piles were built with the same dimensions of the models with the CFA pile. A three-dimensional surface view of the model with steel profile HS1, showing the shape of the undeformed mesh around the pile, is presented in Figure 7c.

Figure 8 compares the experimental and numerical results in terms of horizontal load (H) versus horizontal displacement (y_0) relationships. The lateral load capacities obtained from the field tests are compared with those predicted from the different methods in Table 3.

FHWA [39] proposes tolerable horizontal movements of a single pile of less than 38 mm from a serviceability standpoint. According to AASHTO [40], tolerable displacements of a pile shall be limited to 50 mm or less where vertical displacements are small or to 25 mm or less where combined vertical and horizontal displacements are possible. The ultimate lateral load capacity obtained from the load tests is shown in Table 3 assuming an allowable horizontal displacement $y_0 = 20$ mm as a serviceability limit for the foundation. Since the displacement level of 20 mm was not reached in the tests performed in Area B, the corresponding experimental ultimate loading capacity was obtained from the extrapolation of the curves using the method of Mazurkiewicz [41].

The three-dimensional finite element model closely matched the ultimate lateral capacities to the experimental data (Table 3). The computed ultimate lateral capacity for testing Area A approached the field results closely. The largest discrepancy between numerical and measured results was 21% for H-section pile HS1 embedded in the soil of testing Area B. The 3-D FEM analysis also closely matches the general trend of the experimental curves of CFA and steel H-section piles (Figure 8). Small differences between the three-dimensional numerical simulations and the field results were expected and may be attributed to the variability of soil properties and pile characteristics.

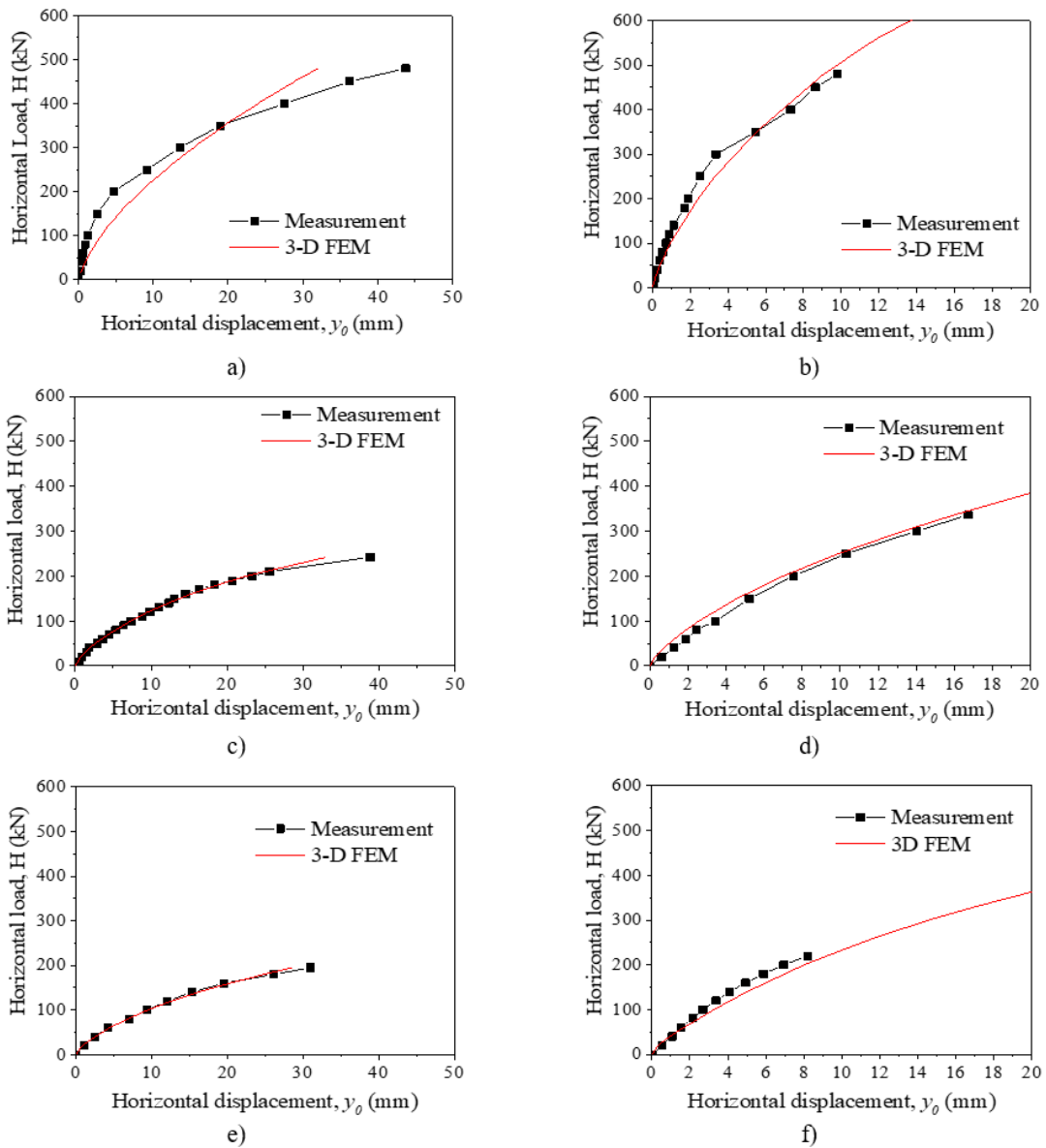


Figure 8. Comparison of the response of laterally loaded piles obtained from field tests and by numerical modelling: (a) CFA pile in Area A; (b) CFA pile in Area B; (c) steel pile HS1 in Area A; (d) steel pile HS1 in Area B; (e) steel pile HS2 in Area A; (f) steel pile HS2 in Area B.

Table 3. Comparison of lateral load capacity of CFA and steel H-section piles obtained from the field tests and the numerical simulations.

Testing Area	Ultimate lateral capacity (kN)		
	Pile type	Field	FEM
A ($D_r = 45\%$)	CFA	355	355
	HS1	188	187
	HS2	162	157
B ($D_r = 70\%$)	CFA	690 ¹	716
	HS1	490 ¹	385
	HS2	312 ¹	362

Note: ¹Values extrapolated according to Mazurkiewicz [41].

Parametric studies were performed to analyze the influence of (i) the soil-pile relative stiffness, (ii) the pile diameter, (iii) the interface friction between pile and soil, (iv) and soil dilatancy (the volume change characteristics of the soil). The analysis of soil-pile relative stiffness was carried out for CFA piles and steel HS1 piles in Areas A and B. Analysis of pile diameter, soil-pile interface friction and soil dilation were developed considering CFA piles only.

Figure 9 shows the response of the steel HS1 pile in Area A for different bending stiffness values ($E_p I_p$), which were varied by changing the Young's modulus of the pile (E_p) while keeping the second moment of inertia (I_p) constant. In Figure 9, $E_p I_p$ is the baseline bending stiffness of profile HS1, which is equal to 56 MNm². Results show that variations in pile stiffness drastically affects the behavior of the pile under lateral loading. Similar trends were also obtained from the parametric analysis carried out with the other pile types embedded in Areas A and B. The results are in accordance with the findings reported by Norris et al. [11], which used the strain wedge (SW) model to predict the behavior of cast-in-place and steel piles in cohesive and cohesionless soils.

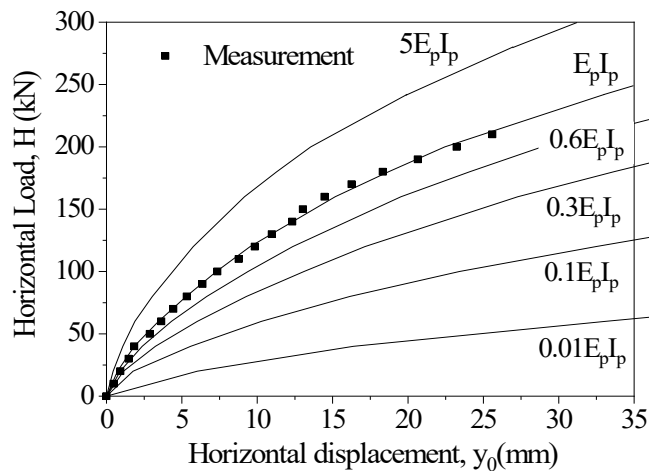


Figure 9. Response of steel H-section pile HS1 embedded in Area A, for various bending stiffness values.

Deeper insight into the effect of pile stiffness can be attained under the framework of soil-pile relative stiffness. Within this concept, the pile and the surrounding soil behave as a single system. The characteristic pile length, T , defined by Equation 2, can be used to determine whether the soil-pile system behaves as a rigid or a flexible member [13], [42]. T is also called relative stiffness factor and expresses a relation between the stiffness of the soil, *i.e.*, the constant of horizontal subgrade reaction (n_h), and the flexural stiffness of the pile ($E_p I_p$). Figure 10 shows the normalized ultimate lateral capacity (H_u^*) as a function of the nondimensional length, given by the ratio between the pile length and the characteristic pile length (L/T). The nondimensional length is another way of quantifying the soil-pile relative stiffness and has the advantage of incorporating the pile length. The larger the nondimensional length, the more flexible the soil-pile system. Data points shown in Figure 10 belong to CFA pile and steel pile HS1 in Areas A and B and were computed for a constant lateral displacement $y_0 = 20$ mm. A trend line fitting the data points is also shown in Figure 10, along with the corresponding empirical equation. H_u^* is expressed as:

$$H_u^* = \frac{H_u}{I_R B^3} \tag{5}$$

where: H_u = ultimate lateral load at a 20-mm lateral displacement, as previously defined; B = pile diameter or width; γ = effective unit weight of the surficial sand layer; I_R = rigidity index of the surficial sand layer, given as [43]:

$$I_R = \frac{G_s}{p' \tan'} \tag{6}$$

where: $G_s = E_s/2(1+\nu_s)$ = shear modulus of the soil; p' = reference pressure, assumed = 100 kPa.

Figure 10 shows that the normalized ultimate lateral capacity H_u^* decreases with increasing soil-pile relative stiffness. At low L/T ratios, a small variation in relative stiffness causes a dramatic variation in H_u^* . Short rigid piles are, therefore, much more influenced by changes in relative stiffness than long flexible members. The effect of soil-pile stiffness becomes much less significant for L/T ratios above 10. $L/T = 4$ has been commonly accepted as the limit beyond which the pile behaves like a long flexible unit [30], [44]. Information presented in Figure 10 can be used in the design of laterally loaded piles in similar local soils for a preliminary estimation of the ultimate lateral capacity.

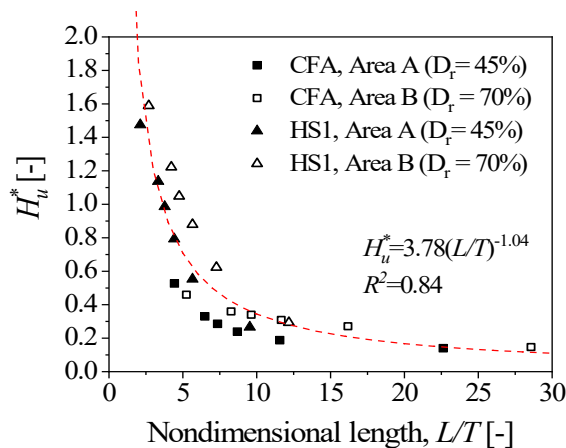


Figure 10. Normalized ultimate lateral capacity of piles H_u^* as a function of the nondimensional length L/T .

The influence of the pile diameter on pile behavior was investigated in the light of the soil-pile relative stiffness concept. The study included the modeling of CFA piles with diameters of 0.3, 0.6, 0.9, and 1.2 m, embedded in Area A. The non-dimensional length ratio (L/T) was maintained unchanged while the pile diameter was varied. Figure 11 shows the effect of the diameter of the pile on the horizontal load (H) for various non-dimensional length ratios (L/T). Linear trend lines were fitted to the data points in Figure 11. Appropriate values of horizontal load were obtained from the calculated $H-y_0$ curve of each corresponding pile and using Equation 1 with the selected characteristic length T . The computational results shown in Figure 11 indicate that the effect exerted by the diameter was significant and became more evident with smaller non-dimensional length ratios. In addition, the relationship between the horizontal load and the pile diameter appears to be nearly linear for the range of examined diameters and non-dimensional length ratios, which agrees with the findings reported by Carter [28], Guo [23], and Kim and Jeong [5].

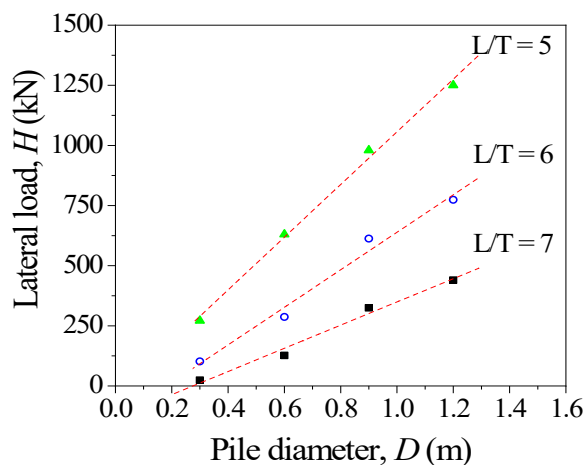


Figure 11. Relationship between lateral load and diameter of CFA piles for various non-dimensional length ratios.

The effect of soil-pile interface friction on the CFA pile response was evaluated by varying the interface strength reduction factor (R_{inter}) within the backfill sand layer. As mentioned previously, R_{inter} is the main controlling parameter of the soil-pile interface in PLAXIS 3D software. The change of the ultimate lateral capacity (H_u) was investigated for strength reduction factors ranging from 0.1 to 0.9, as presented in Figure 12. The computed results reveal that the ultimate lateral capacity presents a non-linear increase with increasing interface property. The influence of R_{inter} on H_u is more relevant between $R_{inter} = 0.1$ to 0.3. Moreover, changes in interface property were comparatively more prominent in Area B, which has the denser surficial backfill sand.

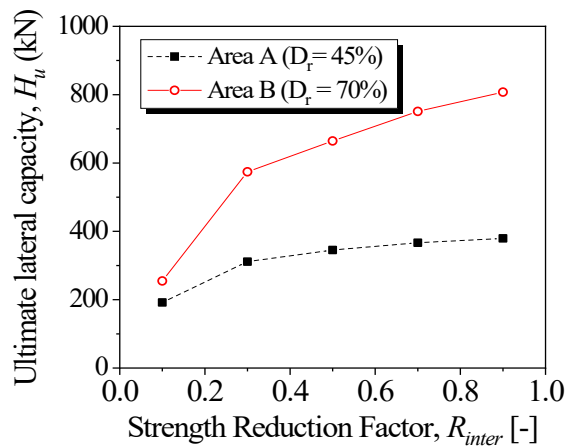


Figure 12. Change of ultimate lateral capacity of CFA piles with interface property.

Shear strength of dense cohesionless soils is largely dependent on volume change properties of the material [45]. The effect of soil dilatancy on soil-pile interaction was assessed by assigning dilatancy angles from 0° to 15° to the backfill sand of both testing areas. Figure 13 shows the variation of the ultimate lateral capacity (H_u) at 20-mm lateral displacement with dilatancy angle (ψ), obtained with the computed data of the CFA pile. The figure shows that soil dilatancy has an influence on pile performance. An increment in the angle of dilatancy from 0° to 15° caused an average 9% increase in the lateral load capacity of the CFA pile. In addition, influence on ultimate lateral capacity is slightly more evident in Area B, which has the denser backfill sand. Comparatively, Choi et al. [15] obtained an increase of 20% in the lateral load capacity of bored piles in weathered granite soil, at a 20-mm lateral displacement, as ψ increased from 0° to 15° .

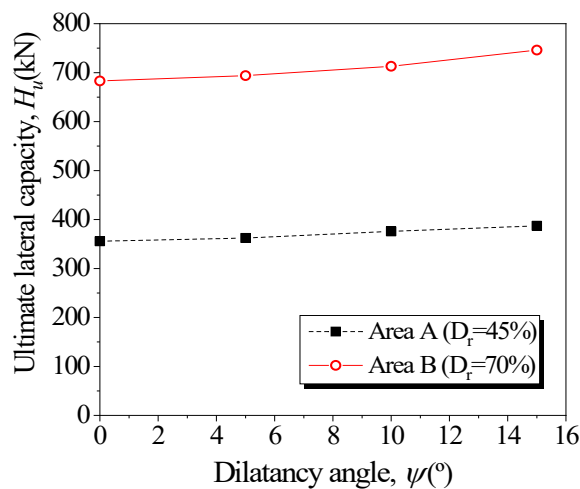


Figure 13. Ultimate lateral capacity of the CFA pile as a function of soil dilatancy.

6 SUMMARY AND CONCLUSIONS

The response of continuous flight auger (CFA) bored piles and steel H-section driven piles to lateral loading was evaluated in this study by field tests and via a three-dimensional finite element (3-D FE) model. The proposed numerical model was substantiated with field tests performed on four CFA piles and eight steel H-section piles in two distinct sandy soil profiles. The three-dimensional finite element approach closely matched the response of CFA and steel H-section piles in terms of the relationships between the applied horizontal load and the horizontal pile displacement recorded from the field tests. A series of parametric analyses was carried out to investigate the role of relevant variables on lateral soil-pile interaction. The main findings of the study can be summarized as follows:

- (1) The pile ultimate lateral load is drastically affected by soil-pile system relative stiffness. Short rigid piles are much more influenced by changes in relative stiffness than long flexible units. The effect of soil-pile stiffness becomes significant for nondimensional length ratios (L/T) below 4.
- (2) Pile diameter exerts a marked effect on pile lateral load, which is more prominent with stiffer soil-pile systems. Moreover, the relationship between horizontal load and pile diameter appears to be nearly linear for the range of examined diameters and nondimensional length ratios.
- (3) The ultimate lateral load capacity of CFA piles significantly increases with increasing soil-pile interface friction coefficient. Soil-pile interface friction affects more the ultimate lateral capacity of piles embedded in denser soils. In addition, variations in ultimate lateral capacity appear to be more significant with lower interface friction coefficients.
- (4) Soil dilatancy causes a slight increase in the ultimate lateral capacity of the CFA piles in the sandy soil deposits. An increment in the angle of dilatancy from 0° to 15° in the surficial sand layer caused an increase of about 9% in the lateral load capacity of the CFA pile for both tested relative densities of 45% and 70%.

ACKNOWLEDGEMENTS

The authors gratefully acknowledge the financial support provided by the National Council for Scientific and Technological Development (CNPq) and the São Paulo Research Foundation (FAPESP - 2018/21573-2). The authors also acknowledge the contributions from João Paulo Costa and Avelino Lourenço on conducting the static lateral loading tests in the field.

REFERENCES

- [1] M. G. Ritter, M. L. Menegotto, M. F. Costella, R. C. Pavan, and S. E. Pilz, "Analysis of soil-structure interaction in buildings with deep foundation," *IBRACON Struct. Mater. J.*, vol. 13, no. 2, pp. 248–260, 2020, <http://dx.doi.org/10.1590/s1983-41952020000200005>.
- [2] L. M. P. Rosa, B. R. Danziger, and E. M. L. Carvalho, "Soil-structure interaction analysis considering concrete creep and shrinkage," *IBRACON Struct. Mater. J.*, vol. 11, no. 3, pp. 564–585, May 2018, <http://dx.doi.org/10.1590/s1983-41952018000300008>.
- [3] E. C. Alves and L. A. Feitosa, "Analysis of the global tall buildings stability in flat slabs considering the soil structure interaction," *IBRACON Struct. Mater. J.*, vol. 13, no. 1, pp. 183–199, Feb 2020, <http://dx.doi.org/10.1590/s1983-41952020000100013>.
- [4] L. M. Gil-Martín, J. F. Carbonell-Márquez, M. A. Fernández-Ruiz, and E. Hernández-Montes, "Theoretical and experimental short-term behavior of non-symmetrical wall pile retaining systems," *Eng. Struct.*, vol. 112, pp. 172–183, Apr 2016, <http://dx.doi.org/10.1016/j.engstruct.2016.01.019>.
- [5] Y. Kim and S. Jeong, "Analysis of soil resistance on laterally loaded piles based on 3D soil-pile interaction," *Comput. Geotech.*, vol. 38, no. 2, pp. 248–257, Mar 2011, <http://dx.doi.org/10.1016/j.compgeo.2010.12.001>.
- [6] P. Michel, C. Butenweg, and S. Klinkel, "Pile-grid foundations of onshore wind turbines considering soil-structure-interaction under seismic loading," *Soil. Dyn. Earthquake Eng.*, vol. 109, pp. 299–311, Jun 2018, <http://dx.doi.org/10.1016/j.soildyn.2018.03.009>.
- [7] A. Nardelli, "The shaft friction degradation of piles under cyclic axial loading in wind turbine foundations," M.S. thesis, Dept. Geotech. Eng., Sch. Eng. Univ. São Paulo, São Paulo, 2019.
- [8] L. Arany, S. Bhattacharya, J. Macdonald, and S. J. Hogan, "Design of monopiles for offshore wind turbines in 10 steps," *Soil. Dyn. Earthquake Eng.*, vol. 92, pp. 126–152, Jan 2017, <http://dx.doi.org/10.1016/j.soildyn.2016.09.024>.
- [9] E. Zacchei, P. H. C. Lyra, and F. R. Stucchi, "Nonlinear static analysis of a pile-supported wharf," *IBRACON Struct. Mater. J.*, vol. 12, no. 5, pp. 998–1009, Oct 2019, <http://dx.doi.org/10.1590/s1983-41952019000500003>.
- [10] L. C. Reese and R. C. Welch, "Lateral loading of deep foundations in stiff clay," *J. Geotech. Eng. Div. ASCE*, vol. 101, no. GT7, pp. 633–649, 1975.
- [11] G. Norris, M. Ashour, and A. Shamsabadi, "Effect of the non-linear behavior of pile material on the response of laterally loaded piles," in *Int. Conf. Recent Adv. Geotech. Earthq. Eng. Soil Dyn.*, 2001, pp. 1–8.

- [12] C. C. Fan and J. H. Long, "Assessment of existing methods for predicting soil response of laterally loaded piles in sand," *Comput. Geotech.*, vol. 32, no. 4, pp. 274–289, Jun 2005, <http://dx.doi.org/10.1016/j.compgeo.2005.02.004>.
- [13] L. C. Reese and W. F. Van Impe, *Single Piles and Pile Groups Under Lateral Loading*, 2nd ed. London: CRC Press, 2011.
- [14] M. A. Almeida, M. G. Miguel, and S. H. C. Teixeira, "Horizontal bearing capacity of piles in a lateritic soil," *J. Geotech. Geoenviron. Eng.*, vol. 137, no. 1, pp. 59–69, Jan 2011., [http://dx.doi.org/10.1061/\(ASCE\)GT.1943-5606.0000410](http://dx.doi.org/10.1061/(ASCE)GT.1943-5606.0000410).
- [15] H.-Y. Choi, S.-R. Lee, H.-I. Park, and D.-H. Kim, "Evaluation of lateral load capacity of bored piles in weathered granite soil," *J. Geotech. Geoenviron. Eng.*, vol. 139, no. 9, pp. 1477–1489, Sep 2013., [http://dx.doi.org/10.1061/\(ASCE\)GT.1943-5606.0000831](http://dx.doi.org/10.1061/(ASCE)GT.1943-5606.0000831).
- [16] L. C. Reese, W. R. Cox, and F. D. Koop, "Analysis of laterally loaded piles in sand," in *Proc. 6th Annu. Offshore Technol. Conf.*, 1974, pp. 473–485.
- [17] American Petroleum Institute, *Recommended Practice 2A-WSD: Planning, Designing and Constructing Fixed Offshore Platforms: Working Stress Design*, 22nd ed. Washington, D.C., 2014.
- [18] H. M. Coyle and R. R. Castello, "New design correlations for piles in sand," *J. Geotech. Eng. Div.*, vol. 107, no. 7, pp. 965–986, 1981.
- [19] K. M. Rollins, R. J. Clayton, R. C. Mikesell, and B. C. Blaise, "Drilled shaft side friction in gravelly soils," *J. Geotech. Geoenviron. Eng.*, vol. 131, no. 8, pp. 987–1003, Aug 2005, [http://dx.doi.org/10.1061/\(ASCE\)1090-0241\(2005\)131:8\(987\)](http://dx.doi.org/10.1061/(ASCE)1090-0241(2005)131:8(987)).
- [20] J. R. Peng, M. Rouainia, and B. G. Clarke, "Finite element analysis of laterally loaded fin piles," *Comput. Struct.*, vol. 88, no. 21–22, pp. 1239–1247, Nov 2010, <http://dx.doi.org/10.1016/j.compstruc.2010.07.002>.
- [21] V. P. Faro, "Carregamento lateral em fundações profundas associadas a solos tratados : concepção, provas de carga e diretrizes de projeto," Ph.D. dissertation, Progr. Pós-grad. Eng. Civ., UFRGS, Porto Alegre, 2014.
- [22] C. E. R. Lautenschläger, "Modelagem numérica do comportamento de fundações profundas submetidas a carregamento lateral," M.S. thesis, Progr. Pós-grad. Eng. Civ., UFRGS, Porto Alegre, 2010.
- [23] W. D. Guo, "Subgrade modulus for laterally loaded piles," in *Proc. Eight Int. Conf. Civ. Struct. Eng. Comput.*, 2001, pp. 273–274, <http://dx.doi.org/10.4203/ccp.73.112>.
- [24] M. Ashour and G. Norris, "Modeling lateral soil-pile response based on soil-pile interaction," *J. Geotech. Geoenviron. Eng.*, vol. 126, no. 5, pp. 420–428, May 2000, [http://dx.doi.org/10.1061/\(ASCE\)1090-0241\(2000\)126:5\(420\)](http://dx.doi.org/10.1061/(ASCE)1090-0241(2000)126:5(420)).
- [25] K. Terzaghi, "Evaluation of coefficients of subgrade reaction," *Geotechnique*, vol. 5, no. 4, pp. 297–326, Dec 1955, <http://dx.doi.org/10.1680/geot.1955.5.4.297>.
- [26] A. B. Vesic, "Beams on elastic subgrade and Winkler's hypothesis," in *Proc. 5th Int. Conf. Soil Mech. Found. Eng.*, 1961, pp. 845–850.
- [27] S. A. Ashford and T. Juirnarongrit, "Evaluation of pile diameter effect on initial modulus of subgrade reaction," *J. Geotech. Geoenviron. Eng.*, vol. 129, no. 3, pp. 234–242, Mar 2003, [http://dx.doi.org/10.1061/\(ASCE\)1090-0241\(2003\)129:3\(234\)](http://dx.doi.org/10.1061/(ASCE)1090-0241(2003)129:3(234)).
- [28] D. P. Carter, "A non-linear soil model for predicting lateral pile response," M.S. thesis, Dept. Civ. Eng., Univ. Auckland, Auckland, New Zealand, 1984.
- [29] J. M. Mabesoone and J. C. Silva, "Geomorphological aspects – sedimentary coastal strip of Pernambuco, Paraíba and part of Rio Grande do Norte," *Geol. Stud.*, vol. Ser. B, no. 10, pp. 117–132, 1991.
- [30] M. T. Davisson, "Lateral load capacity of piles," in *Proc. 49th Ann. Meeting Highw. Res. Board*, 1970, no. 333, pp. 104–112.
- [31] H. Lin, L. Ni, M. T. Suleiman, and A. Raich, "Interaction between laterally loaded pile and surrounding soil," *J. Geotech. Geoenviron. Eng.*, vol. 141, no. 4, 04014119, Apr 2015, [http://dx.doi.org/10.1061/\(ASCE\)GT.1943-5606.0001259](http://dx.doi.org/10.1061/(ASCE)GT.1943-5606.0001259).
- [32] B. H. Fellenius, "Test loading of piles and new proof testing procedure," *J. Geotech. Eng. Div.*, vol. 101, no. GT9, pp. 855–869, 1975.
- [33] Associação Brasileira de Normas Técnicas, *Estacas – Prova de Carga Estática – Método de Ensaio*, ABNT NBR 12131, 2006.
- [34] H. Matlock and L. C. Reese, "Foundation analysis of offshore pile supported structures," in *Proc. 5th Int. Conf. Soil Mech. Found. Eng.*, 1961, pp. 91–97.
- [35] H. G. Poulos and E. H. Davis, *Pile Foundation Analysis and Design*. New York: Wiley, 1980.
- [36] L. Zhang, M. Zhao, and X. Zou, "Behavior of laterally loaded piles in multilayered soils," *Int. J. Geomech.*, vol. 15, no. 2, pp. 06014017, Apr 2015, [http://dx.doi.org/10.1061/\(ASCE\)GM.1943-5622.0000319](http://dx.doi.org/10.1061/(ASCE)GM.1943-5622.0000319).
- [37] S. Prakash and S. Kumar, "Nonlinear lateral pile deflection prediction in sands," *J. Geotech. Eng.*, vol. 122, no. 2, pp. 130–138, Feb 1996, [http://dx.doi.org/10.1061/\(ASCE\)0733-9410\(1996\)122:2\(130\)](http://dx.doi.org/10.1061/(ASCE)0733-9410(1996)122:2(130)).
- [38] T. Schanz, P. A. Vermeer, and P. G. Bonnier, "The hardening soil model: formulation and verification," in *Beyond 2000 in Computational Geotechnics*, R. B. J. Brinkgreve, Ed., Boca Raton: Taylor & Francis, 1999.
- [39] Federal Highway Administration, *Design, Analysis, and Testing of Laterally Loaded Deep Foundations that Support Transportation Facilities*. Washington, D.C.: Fed. Highw. Adm. (Rep. FHWA-HIF-18-031), 2018.

- [40] American Association of State Highway and Transportation Officials, *Standard Specifications for Highway Bridges*, 17th ed. Washington, D.C., 2002.
- [41] B. K. Mazurkiewicz, *Test Loading of Piles According to Polish Regulations* (Prel. Rep. 35). Stockholm: Swedish Academy of Eng. Sciences, 1972.
- [42] B. B. Broms, "Lateral resistance of piles in cohesionless soils," *J. Soil Mech. Found. Div.*, vol. 90, no. 3, pp. 123–156, 1964.
- [43] A. S. Vesic, "Bearing capacity of shallow foundations," in *Foundation Engineering Handbook*, 1st ed., H. F. Winterkorn and H. Y. Fang, Eds., New York, NY: Van Nostrand Reinhold, 1975, pp. 121–147.
- [44] M. J. Tomlinson, *Pile Design and Construction Practice*, 4th ed. London: E & FN Spon., 1994.
- [45] M. D. Bolton, "The strength and dilatancy of sands," *Geotechnique*, vol. 36, no. 1, pp. 65–78, Mar 1986, <http://dx.doi.org/10.1680/geot.1986.36.1.65>.

Author contributions: AMDS: numerical analyses, manuscript editing and review; YDJC: conceptualization, funding acquisition, supervision, analysis of results and writing; AGDA: experimental analyses; CMLC: supervision and manuscript review.

Editors: Mark Alexander, Guilherme Aris Parsekian.